

KINEMATICS AND MORPHOLOGY OF IONIZED GAS IN HICKSON COMPACT GROUP 18

H. PLANA^{1,2}

Observatorio Astronomico Nacional, UNAM, Apartado Postal 877, 22800, Ensenada, BC, Mexico

P. AMRAM²

IGRAP, Observatoire de Marseille, 2 Place Le Verrier, 13248 Marseille Cedex 04, France

C. MENDES DE OLIVEIRA³

Instituto Astronômico e Geofísico (IAG), Av Miguel Stefano 4200 CEP: 04301-904 São Paulo, Brazil

AND

C. BALKOWSKI⁴

Observatoire de Paris, DAEC, UMR 8631, CNRS et Université Paris 7, F-92195 Meudon Cedex, France

To appear in Astronomical Journal

ABSTRACT

We present new observations of $H\alpha$ emission in the Hickson Compact Group 18 (HCG 18) obtained with a scanning Fabry-Perot interferometer. The velocity field does not show motions of individual group members but, instead, a complex common velocity field for the whole group. The gas distribution is very asymmetric with clumps of maximum intensity coinciding with the optically brightest knots. Comparing $H\alpha$ and HI data we conclude that HCG 18 is not a compact group but instead a large irregular galaxy with several clumps of star formation.

Subject headings: galaxies: irregular — galaxies: evolution — galaxies: formation — galaxies: individual (UGC 2140) — galaxies: interactions — galaxies: ISM — galaxies: kinematics and dynamics — instrumentation: interferometers

1. INTRODUCTION

Compact groups of galaxies have been known for over 30 years (Vorontsov-Vel'yaminov 1959, Arp 1966, Rose 1977, Hickson et al. 1977, Hickson 1982). A spectroscopic survey confirmed that 92 of the 100 groups catalogued by Hickson (1982) have at least three accordant redshift members with 69 groups having at least four (Hickson et al. 1992). With a median galaxy-galaxy separation of $40 \text{ h}^{-1} \text{ kpc}$ and a low typical velocity dispersion ($\sigma \sim 200 \text{ km s}^{-1}$, Hickson et al. 1992), compact groups are usually considered to be ideal laboratories for studying galaxy interactions. The most direct way to determine if interactions have occurred among group galaxies is to measure their kinematics in order to check if they are disturbed or normal. Study of the ionized gas kinematics for several of the Hickson group galaxies has shown that they are in different evolutionary stages (Mendes de Oliveira et al. 1998, Plana et al. 1998).

HCG 18 (H18, Arp 258 or VV 143) was cataloged by Hickson (1982) as a group of three irregular galaxies (H18b, c and d with radial velocities between 4080 and 4163 km s^{-1}) plus one discordant-redshift S0 galaxy (H18a with a velocity of 10000 km s^{-1} ; Hickson 1993). In this paper the H18 group refers to the triplet H18b, c and d.

Verdes-Montenegro et al. (1998) determined the IRAS flux for H18d and upper limits on the flux for H18b and H18c. They also determined the H_2 mass for H18b and H18c, from their CO observations. Allam et al. (1996) also give IRAS flux but for H18b, c and d together. We eventually use Allam's values because H18 IRAS emission can not be spatially resolved. HI data is also available for this group, besides the optical measures (Hickson 1993). From a study of the HI velocity field of the group Williams and van Gorkom (1988, hereafter W&vG) concluded that

the HI gas is concentrated in a single cloud with $m_{\text{HI}} = 10^{10} M_{\odot}$ encompassing all of the optical structures.

We observed the H18 group in the $H\alpha$ emission line with a scanning Fabry-Perot instrument and we obtained velocity and $H\alpha$ integrated flux maps for the system. This observation is part of a larger program that has the goal of unveiling kinematic evidences of interactions in compact groups of galaxies in order to determine their evolutionary stages.

H18 appears to be one of the most complex groups of the Hickson sample. A key question raised by the HI study of W&vG was the nature of the three components b, c and d, namely if they are individual entities or form one single galaxy. Based on our observations and comparisons between our data and the HI results, we conclude that H18 is likely to be a single large irregular galaxy. The $H\alpha$ maps presented in this study permit the determination of the $H\alpha$ luminosity ($L(H\alpha)$) and star formation rate (SFR) of the system, which can be compared with typical values for samples of irregular galaxies studied by Hunter et al. (1986, 1989 and 1993). We also compare the total B luminosity (L_B) of the group and its far-infrared luminosity (L_{FIR}) with values given in the literature for typical irregular galaxies.

The paper is organized as follows. Section 2 gives details about the reduction of the Fabry-Perot data. Section 3 describes the results. Section 4 has a comparison of our results with the HI observations. Section 5 presents a discussion about the nature of H18 in light of our new $H\alpha$ observations and section 6 contains our summary and final remarks.

2. OBSERVATIONS AND DATA REDUCTION

TABLE 1
JOURNAL OF PEROT-FABRY OBSERVATIONS

Compact Group of Galaxies Hickson 18		
Observations	Telescope	CFHT 3.6m
	Equipment	MOS/FP @ Cassegrain focus
	Date	August, 22th 1996
	Seeing	$< 1''$
Interference Filter	Central Wavelength	6653 \AA^1
	FWHM	23 \AA^2
	Transmission (maximum)	0.6
Calibration	Neon Comparison light	$\lambda 6598.95 \text{ \AA}$
Perot-Fabry	Interference Order	1162 @ 6562.78 \AA
	Free Spectral Range at $H\alpha$	265 km s^{-1}
	Finesse at $H\alpha$	12
Sampling	Spectral resolution at $H\alpha$	27344 at the sample step
	Number of Scanning Steps	24
	Sampling Step	$0.24 \text{ \AA} (11 \text{ km s}^{-1})$
	Total Field	$430'' \times 430'' (500 \times 500 \text{ px}^2)$
Detector	Pixel Size	$0.86''$
		STIS 2 CCD
Exposures times	Total exposure	2 hours
	Total exposure time per channel	300s

¹ For a temperature de 5° . ² For a mean beam inclination of 2.7° .

Observations were carried out in August 1996 with the multi-object spectrograph focal reducer in Fabry-Perot mode attached to the F/8 Cassegrain focus of the 3.6m Canada-France-Hawaii telescope (CFHT). The CCD was a STIS 2 detector, 2048×2048 pixels with a read-out noise of 9.3 e^- and a pixel size on the sky of $0.86''$ after 2×2 binning. Table 1 contains the journal of observations. Reduction of the data cubes were performed using the CIGALE/ADHOC software (Boulesteix 1993). The data reduction procedure has been extensively described in Amram et al. (1996).

Wavelength calibration was obtained by scanning the narrow Ne 6599 \AA line under the same conditions as the observations. Velocities measured relative to the systemic velocity are very accurate, with an error of a fraction of a channel width ($< 3 \text{ km s}^{-1}$) over the whole field.

Subtraction of bias, flat fielding of the data and cosmic-ray removal have been performed for each image of the data cube. To minimize seeing variation, each scan image was smoothed with a gaussian function of full-width at half maximum equal to the worse-seeing data of the data cube. Transparency and sky foreground fluctuations have also been corrected using field star fluxes and galaxy-free windows.

The signal measured along the scanning sequence was separated into two parts: (1) an almost constant level produced by the continuum light in a 23 \AA passband around $H\alpha$ (continuum map), and (2) a varying part produced by the $H\alpha$ line ($H\alpha$ integrated flux map). The continuum level was taken to be the mean of the three faintest chan-

nels, to avoid channel noise effects. The $H\alpha$ integrated flux map was obtained by integrating the monochromatic profile in each pixel. The velocity sampling was 11 km s^{-1} . The $H\alpha$ integrated flux map had one-pixel resolution in the positions of H18b, H18c and H18d. Spectral profiles were binned in the outer parts to 5×5 pixels in order to increase the signal-to-noise ratio. Strong OH night sky lines passing through the filters were subtracted by determining the level of emission away from the galaxies (Laval et al., 1987).

A rough flux calibration was attempted using the group HCG 100 observed during two runs (1995 at the ESO 3.6m and 1996 at the CFHT). Monochromatic images of HCG 100 have been calibrated in flux using the Cartwheel Galaxy, observed during the 1995 ESO run (see Amram et al. 1998 for details). We then determined the HCG 18 galaxy fluxes relative to HCG 100. We have reasonable agreement with fluxes published by Iglesias-Parámo & Vílchez 1999 for H100a and H100b. We compared our H18 fluxes with those determined by Laurikainen and Moles (1989) and we found a value that was four times higher for the flux of H18d and around five times for H18b (they did not measure the flux of the H18c). Difference by factors of four or five can be understood if we note that flux calibration with slit observations can significantly underestimate the true flux. $H\alpha$ profiles for the H18 galaxies were measured to a minimum flux density of $1.1 \times 10^{-16} \text{ erg s}^{-1} \text{ cm}^{-2} \text{ arcsec}^{-2}$ and a maximum of $9.3 \times 10^{-15} \text{ erg s}^{-1} \text{ cm}^{-2} \text{ arcsec}^{-2}$ (corresponding to a S/N between 3 and 500).

TABLE 2
PHYSICAL PARAMETERS

	HCG 18b	HCG 18c	HCG 18d
Other names	UGC 2140a Arp 258 / VV 143	UGC 2140b Arp 258 / VV 143	UGC 2140c Arp 258 / VV 143
α (1950) ¹	02 ^h 36 ^m 18.5 ^s	02 ^h 36 ^m 18.2 ^s	02 ^h 36 ^m 17.0 ^s
δ (1950) ¹	18°10'04.1"	18°10'24.5"	18°10'43.9"
Morphological type (Hickson) ¹	Im	Im	Im
B_{TC} ¹	14.90	15.61	15.10
Systemic heliocentric velocity/ ¹ (km s ⁻¹)	4082 ± 40	4163 ± 37	4067 ± 58
Gas central velocity (km s ⁻¹)	4063 ± 20	4108 ± 20	4061 ± 20
D(Mpc) ²	54	54	54
HI velocities/ ² (km s ⁻¹)	4065	4085	4095
FWHM of central profiles (km s ⁻¹)	65 ± 20	70 ± 20	80 ± 20

¹ Hickson 1993 ² Williams & van Gorkom 1988

3. RESULTS

We obtained H α integrated flux map and velocity maps for H18b, c and d. The systemic velocity of H18a was outside of the range of the interference filter we used. Fig. 1 shows continuum isophotes superimposed on a DSS image.

3.1. Fabry-Perot interferograms and channel maps

Fig. 2 presents channel maps for H18 with a field-of-view of is 1.8' x 1.8'. The velocity amplitude is low, with the lowest-velocity channel at 4003 km s⁻¹ and the highest-velocity channel at 4177 km s⁻¹. The optical centers of H18b, c and d are represented by crosses. Several emission-line regions appear, with velocities between 4003 km s⁻¹ and 4068 km s⁻¹ south of the principal optical continuum sources. We can clearly see from channels 4047 to 4090 km s⁻¹ that H18c and d have a common emission. North of the group there is another emission-line region which appears between channels 4068 - 4177 km s⁻¹. Starting at channel 4025 km s⁻¹, the emission for H18d gets continuously stronger, until it reaches channel 4090 km s⁻¹. There are optical counterparts for almost all emission-line regions except the ones between 4003 - 4068 km.s⁻¹. The southern regions between 4003 and 4047 km.s⁻¹, form a circular pattern. Looking carefully at optical images (Hickson 1993; Arp 1966) reveals faint optical counterparts to the southern sources. This circular structure does not show any evidence for expansion. Examination of HI channel maps (W&vG), reveals that the southern emitting regions coincide with HI emission in the range 4015-3994 km.s⁻¹.

The extended H α emission of H18 is not concentrated in a single cloud but instead shows substructures. As described in detail below, we do not detect rotation for individual group members. Except for the southern and northern clumps, all the other emission-line regions are aligned along a position angle of $\sim 160^\circ$.

3.2. Velocity field and line-of-sight velocity curves

Figure 3 presents the velocity field for the H18b, c and d system. H α intensity isophotes are superimposed on the velocity field. The total extent of the velocity mapped structure is $\sim 2.2'$ by $30''$. The radial velocity across the map varies from 4007 km s⁻¹, in the southern region, to 4127 km s⁻¹, in the northern and northeastern part of the group. This map shows that there is no circular motion for the group as a whole. Nevertheless, the southern region seems to have an independent kinematics from the rest of the group.

Line-of-sight (LOS) velocity curves (uncorrected for inclination) can be derived from the velocity field. Fig. 4 shows LOS velocity curves along different position angles. Fig. 4a presents the LOS velocity diagram for the southern region, with a cut along PA $\sim 80^\circ$ (see Fig. 1 for the exact location). Fig. 4b presents the LOS velocity curve for the group as a whole, along a PA $\sim 160^\circ$, the PA that best describes the velocity field of the group.

The first plot (Fig. 4a) shows disk-like rotation with a velocity amplitude of 70 km s⁻¹ and an almost solid body motion across a region of $20''$. This plot includes all points within a cone of half radius 20 degrees. The emission is rather weak in comparison with the rest of the system. The measured profiles have a S/N ratio between five and ten. In this region there are no catalogued members noted by Hickson (1982). This clear velocity gradient may indicate an independent motion for the southern part of the system.

Fig. 4b shows the velocity curve along a PA $\sim 160^\circ$, which is our best estimate for the PA of the major axis of the entire group. For this plot we show the average velocity values with error bars (calculated in a two pixels crown) inside a cone of 20° half-radius. We note that although there is a large scatter in the velocities (with a dispersion of ± 20 km s⁻¹), there is a clear velocity gradient from the northwest to the southeast of the group, of mean total amplitude of 78 km s⁻¹, over 90 arcsec. We marked on

Fig. 4b the positions of the three group members, H18b, c and d.

3.3. Monochromatic emission

Fig. 5 shows isophotes of averaged $H\alpha$ flux (superimposed on the DSS image) obtained by integrating the emission above the continuum. The image was smoothed with a box of 5×5 pixels. The threshold is 10^{-16} and the step is $5 \times 10^{-16} \text{ erg s}^{-1} \text{ cm}^{-2} \text{ arcsec}^{-2}$. The total $H\alpha$ flux is $2.5 \times 10^{-12} \text{ erg s}^{-1} \text{ cm}^{-2}$. Using the formula of Osterbrock (1974) and assuming an electronic density of 1000 cm^{-3} , we obtain an upper limit for the ionized gas mass of $M_{HII} = 2 \times 10^6 M_{\odot}$. The five compact emitting regions seen in Fig. 5 represent more than 50% of the total emission from the source. As mentioned before, although the gas emission is clumpy, the profiles are continuous between H18c and H18d. We also note that regions 2 and 5 do not correspond to any cataloged group members (Hickson 1993) although we do detect counterparts for these emission regions in our continuum image.

3.4. Star Formation History of HCG18

Total $H\alpha$ flux implies a luminosity $L(H\alpha) = 2.2 \times 10^8 L_{\odot}$ adopting a distance of 54 Mpc for H18 (with $H_0 = 75 \text{ km.s}^{-1} \text{ Mpc}^{-1}$).

The visual B magnitude in Hickson (1993), yields a B luminosity of $L(B) = 1.1 \times 10^{10} L_{\odot}$.

From Allam et al. (1996) IRAS fluxes we derive the total FIR luminosity of $L(\text{FIR}) = 2.42 \times 10^9 L_{\odot}$ for the whole group.

The multiwavelength luminosities (B, $H\alpha$, FIR) can be used to determine the star formation rates (SFR) for different epochs in the galaxy history. Table 3 summarizes the different quantities derived for H18. A recent SFR can be estimated from the B luminosity and equation 7 in Gallagher et al. (1984b). This equation represents the average SFR over the lifetime of the stars which dominate the blue light ($0.4 - 6 \times 10^9$ years). We then estimate $\text{SFR}(B) = 0.29 \times 10^{-10} L_B M_{\odot} \text{ yr}^{-1}$ (where L_B is the bolometric solar luminosities). And $\text{SFR}(B) = 0.32 \times M_{\odot} \text{ yr}^{-1}$. The current SFR can be deduced from both FIR ($L(\text{FIR})$) and $H\alpha$ ($L(H\alpha)$) luminosities. The current SFR is driven by the number of OB stars. Knowledge of the FIR luminosity may measure this (through the dust heated by OB stars). But our lack of understanding of the details of the radiation processes responsible for the FIR luminosity introduces uncertainties in the calculation of the recent SFR (Gallagher & Hunter 1987). The major assumption for the recent SFR determined using $L(\text{FIR})$ is the role played by the massive stars in heating the dust. Thronson & Telesco (1986) adopted an $\text{SFR}(\text{IR}) = 6.5 \times 10^{-10} L(\text{FIR}) M_{\odot} \text{ yr}^{-1}$ (with $L(\text{FIR})$ in L_{\odot}) giving the current SFR over 2×10^6 years. Under similar assumptions but using a different stellar luminosity law and different upper mass limits, Gallagher & Hunter (1987) deduced another formula which give rates that are half the values calculated by Thronson & Telesco (1986) (for a given luminosity).

The $H\alpha$ luminosity provides another way to estimate the current SFR (Hunter & Gallagher 1986, Gallagher & Hunter 1987), by calculating the flux of Lyman continuum photons from hot young stars. In that case, a problem could arise from the effect of dust extinction and the

model chosen to convert the observed $L(H\alpha)$ to Lyman count luminosity (Gusten & Mezger 1982). Hunter & Gallagher (1986) adopted, $\text{SFR}(H\alpha) = 7.02 \times 10^{-42} L(H\alpha) M_{\odot} \text{ yr}^{-1}$, with $L(H\alpha)$ in erg s^{-1} . We found a $\text{SFR}(\text{FIR}) = 1.58 M_{\odot} \text{ yr}^{-1}$ and $\text{SFR}(H\alpha) = 6.1 M_{\odot} \text{ yr}^{-1}$ for H18. The factor of four difference between the measurements. However, is expected given the assumptions made in the calculations.

4. COMPARISON WITH HI DATA

HI data (W&vG) represents an important piece of information for understanding the nature of H18. They presented HI velocity field and integrated images for H18 and suggested that it is a single giant cloud ($3.0' \times 2.5'$) not associated with any individual member of the group. They found evidence for systematic rotation along a position angle of 20° and velocities amplitude from 150 km s^{-1} . Inspection of their Fig. 3, which presents the HI velocity field of the group, shows a variation of the kinematic position angle along the major axis of the velocity field.

In order to compare W&vG's data with the $H\alpha$ kinematics we performed a gaussian smoothing of our data cube with $\text{FWHM} = 22''$. In order to check for possible smoothing artifact due to very bright region (H18d), we normalized the ionized gas data cube and found no contamination was present. Fig. 6 shows the resultant $H\alpha$ velocity field superimposed on the HI velocity field for comparison. The velocity amplitude is between 170 km s^{-1} , consistent with the HI velocity range.

The two velocity fields present similarities and differences. The global appearance of the $H\alpha$ velocity field appears to be less regular than that for the HI. The $H\alpha$ map shows a region of low velocities coinciding with H18d and not present in HI.

The southern part of the $H\alpha$ and HI velocity fields are similar. In this region the HI velocities range from $4020 - 4050 \text{ km s}^{-1}$ while the $H\alpha$ velocities go from 4037 km s^{-1} to 4072 km s^{-1} .

The HI and $H\alpha$ velocity fields show less the agreement in the northern part of H18. In the center, at the 4050 km s^{-1} , the PA of the major axis of the $H\alpha$ velocity field is close to $0 \pm 5^\circ$ while it is close to $20 \pm 5^\circ$ for HI. In the northern part, the morphology of the two maps is different mainly due to the presence of the low velocity region to the west of the $H\alpha$ velocity field. In the northeast, where the influence of the low velocity region is not visible, the coincidence with the HI isovelocitys is better.

Fig. 4c presents the LOS velocity diagram constructed from the smoothed velocity field at $\text{PA} = 20^\circ$. The center was chosen to coincide with H18c. We also include the data points from W&vG derived from their Fig 3. Our velocity amplitude $\sim 150 \text{ km s}^{-1}$ but the rotation while systematic is obviously not axisymmetric. The HI velocities, in comparison suggest a solid-body rotation. The velocity amplitude is close to the value found by us and the gradient is slightly steeper.

5. DISCUSSION – THE NATURE OF H18

The nature of H18 in light of HI observations was discussed by W&vG. They considered two possibilities for the nature of this system: 1) it is a knotty irregular galaxy

TABLE 3
DERIVED DATA

HCG 18	
$F(H\alpha) \text{ erg s}^{-1} \text{ cm}^{-2}$	$2.5 \cdot 10^{-12}$
$L(H\alpha) L_{\odot}$	$2.2 \cdot 10^8$
$L(B) L_{\odot}$	$1.1 \cdot 10^{10}$
$L(FIR) L_{\odot}$	$2.4 \cdot 10^9$
$SFR(H\alpha) M_{\odot} \text{ yr}^{-1}$	6.1
$SFR(B) M_{\odot} \text{ yr}^{-1}$	0.32
$SFR(FIR) M_{\odot} \text{ yr}^{-1}$	1.58
M_{HI}/M_{HII}	5000
$M_{HI}/L(B) M_{\odot} / L_{\odot}$	0.9

(hereafter referred to as “the irregular-galaxy scenario”), or 2) it is an interacting group and the observed HI cloud is a remnant of an interpenetrating collision which stripped the gas from the colliding galaxies. Our data and analysis confirm the first scenario.

5.1. Arguments in favour of the irregular-galaxy scenario

The strongest argument in favour of H18 being an irregular galaxy comes from the kinematics of the HI and H α gas. The velocity maps show velocity amplitudes of $\pm 70 \text{ km s}^{-1}$ and gradients of $15 \text{ km s}^{-1} \text{ kpc}^{-1}$ for the ionized gas and $10 \text{ km s}^{-1} \text{ kpc}^{-1}$ for the HI. These confirm that H18 is a slow rotator. The few detailed studies concerning the kinematics concerning irregular galaxies (Hunter 1982, Tomita et al. 1998) confirm that irregular galaxies are indeed slow rotators.

Hunter (1982) studied a sample of 15 irregular galaxies, five of which showed velocity gradients between 60 and $80 \text{ km s}^{-1} \text{ kpc}^{-1}$, consistent with results found for H18. Tomita et al. (1998) produced position–velocity diagrams for four dwarf galaxies along several slit orientations. They did not detect disk-like rotation but velocity gradients were clearly seen. They also found a velocity difference of 10 to 20 km s^{-1} between the HII regions and the HI gas disk. Saito et al. (1992) reported a kinematic study of the ionized gas in IC 10 and, particularly, a comparison between the ionized and HI gas kinematics for this galaxy giving the same kind of velocity differences that we found for H18. Two other works have studied a few irregular galaxies with a Fabry Perot interferometer. Sasaki et al. (1997) reported observations of NGC 4449 and its H α velocity field that show a kpc-scale mosaic structure of blueshift and redshift components with a slow global rotation. They confirmed the counter rotation between ionized gas and the HI halo for this galaxy. Rosado et al. (1998) and Valdez & Rosado (1998) present an optical velocity field for NGC 4449 showing a decreasing gradient along the optical bar and an anticorrelation with respect to the HI velocity field.

The LOS velocity curve of the southern part (Fig. 4a) suggests an independent disk rotation. The velocity curve along the major axis of H18 (Fig 4b) shows that H18b and c lie on the curve, suggesting that they are gravitationally

bound.

The ratio $L_B/L(H\alpha)$ of H18 is consistent with the irregular-galaxy hypothesis. Hunter et al. (1989) find a value for the ratio $L_B/L(H\alpha) \sim 44$, for giant irregular galaxies while we find 50 for H18.

One last piece of evidence for the irregular-galaxy scenario comes from the HI data. The size of the large HI cloud around H18 measured by W&vG and the total HI mass they found ($M(HI)=10^{10} M_{\odot}$) are consistent with values found for HI clouds around irregular galaxies such as IC 10 (Shostak & Skillman 1989) and NGC 4449 (Hunter et al. 1998). Normalized by the total B luminosity the HI total mass also compares with the typical values found for the Hunter (1993) sample.

5.2. Differences between H18 and irregular galaxies

The main difference between H18 and irregular galaxies concerns the FIR properties and star formation rates. Hunter et al. (1989, 1993) present properties (in FIR, H α and broad band imaging) for a sample of 43 irregular galaxies of different types (dwarf, giants, distant, amorphous). We used their sample of dwarf and giant irregular galaxies as a control sample for comparison with the properties of H18.

We measured ratios of $L(FIR)/L_B = 0.22$ and $L(FIR)/L(H\alpha)=11$ for H18. The $L(FIR)/L_B$ ratio is significantly lower than the mean value of 1.9 and 1.0 found for Hunter et al.’s (1989) sample of giant and dwarf irregulars respectively (the two other classes, “amorphous” and “distant”, show much larger ratios). The $L(FIR)/L(H\alpha)$ ratio is also lower than the mean values of 90 and 71 for the giant and dwarf irregulars respectively. However, within each subclass, giant, dwarf, amorphous and distant, there is significant scatter in the ratios. We also derived a dust temperature for H18 (from the S(100 μ) and S(60 μ) IRAS data) of $T_d=27\text{K}$, which is cooler than typical dust temperatures derived for other irregular galaxies.

The recent SFR ($SFR(B)$) and the current SFR ($SFR(FIR)$ or $SFR(H\alpha)$) are much higher (by one or two orders of magnitude) compared with values from Hunter et al’s sample. If, however, we calculate a SFR per area, using the $SFR(H\alpha)$ and taking the area to be that enclosed within the ellipse of major and minor axes defined by the

H α integrated flux map (Fig.5), we find that the SFR/area is $5 \times 10^{-9} \text{ M}_{\odot} \text{ yr}^{-1} \text{ pc}^{-2}$. Hunter & Gallagher (1986) have a similar average for the SFR/area for the giant irregular galaxies of their sample. The other subclasses of irregular galaxies have average values for the SFR/area ratio that are slightly lower than that found for H18.

6. SUMMARY AND FINAL REMARKS

HCG 18 is a special case in the Hickson compact group catalogue (Hickson, 1982). It was originally thought to be a group composed of three members, H18b, c and d and a discordant-redshift galaxy, H18a. The three members are not well separated and they are embedded in a diffuse halo. A key question raised by W&vG was about the nature of H18. Our H α observations suggest that H18 is in fact a giant irregular galaxy confirming previous HI results.

Evidence in favour of the irregular-galaxy scenario here. We find that the blobs (previously called galaxies, when the system was classified as a group) are kinematically connected and therefore they may form a single object. We find a velocity gradient similar to what was found by W&vG from the HI data and consistent with values for irregular galaxies. A comparison between the H α and the HI velocity fields shows a difference on their morphologies but the velocity amplitudes and gradients are similar. Various authors also show differences between the HI and the optical kinematics for other irregular galaxies (see Section

5.1). The H α emission shows that the ionized gas distribution is clumpy which is rather common for irregular galaxies. The values for the total luminosities in B, H α and FIR are larger than those for the Hunter et al.'s sample (1989) of irregular galaxies but if we normalize the L(H α) by the total B luminosity or the L(FIR) by the total B luminosity, it appears that the ratios are close to what other authors find for giant irregular galaxies. The inferred star formation rate of H18 is higher than the average for irregular galaxies although the values are comparable when they are normalized by the area of the galaxies.

Two others groups that may be classified as a single object, an irregular galaxy, are HCG 31 and HCG 54. H54 is formed by three members classified as irregulars and one late spiral and H31 is formed of four members, a and c seems to be a single object. Kinematical study is necessary to confirm if it is an irregular galaxy like H18. If true, this would suggest that only a small fraction ($\sim 3\%$) of catalogues of compact groups may be misclassified single objects.

The authors would like to thank the CFHT staff for helping during the observations and Drs. R. Sancisi, M. Moles, D.A Hunter and the anonymous referee for helpful discussions and corrections. H. Plana acknowledges the financial support of the Brazilian FAPESP, under contract 96/06722-0 and the Mexican CONACYT.

REFERENCES

- Allam S., Assebdorp R., Longo G., Braum M., Richter G., 1996, A&AS 117, 39
 Amram P., Balkowski C., Boulesteix J., Cayatte V., Marcelin M., Sullivan W. 1996, A&A 310, 737
 Amram P., Mendes de Oliveira C., Boulesteix J., Balkowski C., 1998, A&A 330, 881
 Arp H. 1966, ApJ Suppl. 14, 1
 Boulesteix J., 1993, "ADHOC reference manual", Publications de l'Observatoire de Marseille
 de Vaucouleur G, de Vaucouleur A, Corwin H. 1976 Second Reference Catalog of Bright galaxies (Austin: University of Texas Press).
 Gallagher J.S., Hunter D.A., 1984a, Ann. Rev. Astron. Astrophys. 22, 37
 Gallagher J.S., Hunter D.A., Tutukov A.V., 1984b, ApJ 284, 544
 Gallagher J.S., Hunter D.A., 1987, in Star Formation in Galaxies, ed C. Persson (NASA CP-2466) p167
 Gusten R. & Mezger P.G. 1982 Vistas in Astro. 26, 159
 Hickson P., Richstone D. O., Turner E. L., 1977, ApJ 213, 323
 Hickson P., 1982, ApJ, 255, 382
 Hickson P., Mendes de Oliveira C., Huchra J.P., Palumbo G.G.C., 1992, ApJ 399, 353
 Hickson P., 1993, Astrophys. Letters & Communications Vol. 29 numbers 1-3
 Hunter D.A. 1982 ApJ 260, 81
 Hunter D.A., Gallagher III J.S., 1986 PASP 98, 599
 Hunter D.A., Gallagher III J.S., Rice W.L., Gillet F.C., 1989 ApJ 336, 152
 Hunter D.A., Hawley W.N., Gallagher III J.S., 1993 AJ 106, 1797
 Hunter D.A., Wilcots E.M., van Woerden H., Gallagher J.S., Khole S., 1998, ApJ Letters 495, L47
 Iglesias-Parámo J., Vílchez J.M., 1999 ApJ 518, 94
 Laurikainen E., Moles M., 1989 ApJ 345, 176
 Laval A., Boulesteix J., Georgelin Y.P., Georgelin Y.M., Marcelin M., 1987, A&A, 175, 199
 Mendes de Oliveira C., Plana H., Amram Ph., Bolte M., Boulesteix J., 1998 ApJ 507, 691
 Osterbrock D.E., 1974, Astrophysics of Gaseous Nebulae (W.A. Freeman and Company, San Francisco) p 71
 Plana H., Mendes de Oliveira C., Amram Ph., Boulesteix J., 1998 AJ 116, 2123
 Rosado M., Valdez M., Bullesos A., Esteban C., Georgiev L., Borissova J. 1998a in IAU Symposium 190 New Views of the Magellanic Clouds, in press
 Rose J.A., 1977, ApJ 211, 311
 Saito M., Sasaki M., Ohta K., Yamada T., 1992 PASP, 44 593
 Sasaki M., Ohtani H., Saito M., Ohta K., Yoshida M., Shimizu Y., Koyano H., Kosugi G., Aoki K., Sasaki T., 1997 in Dwarf Galaxies: Probes for Galaxy Formation and Evolution Joint Discussion 2.
 Shostak G.S., Skillman E.D., 1989, A&A 214, 33
 Thronson H.A., Telesco C.M., 1986, ApJ 311, 98
 Tomita A., Ohta K., Nakanishi K., Takeuchi T., Saito M., 1998, ApJ 116, 131
 Valdez M., Rosado M. 1998 in IX Latin American Regional IAU Meeting. Ed Aguilar L. Carraminana A. Revista Mexicana de Astronomia y Astrofisica Serie de Conferencias in press
 Verdes-Montenegro L., Yun M.S., Perea J., del Olmo A., Ho P.T.P., 1998 ApJ 497, 89
 Vorontsov-Vel'yaminov, B.A. 1959, Atlas and Catalog of Interacting Galaxies Vol 1 Sterberg Institute, Moscow State University, Moscow
 Williams B.A., van Gorkom J.H., 1988 AJ 95, 352 (W&vG)

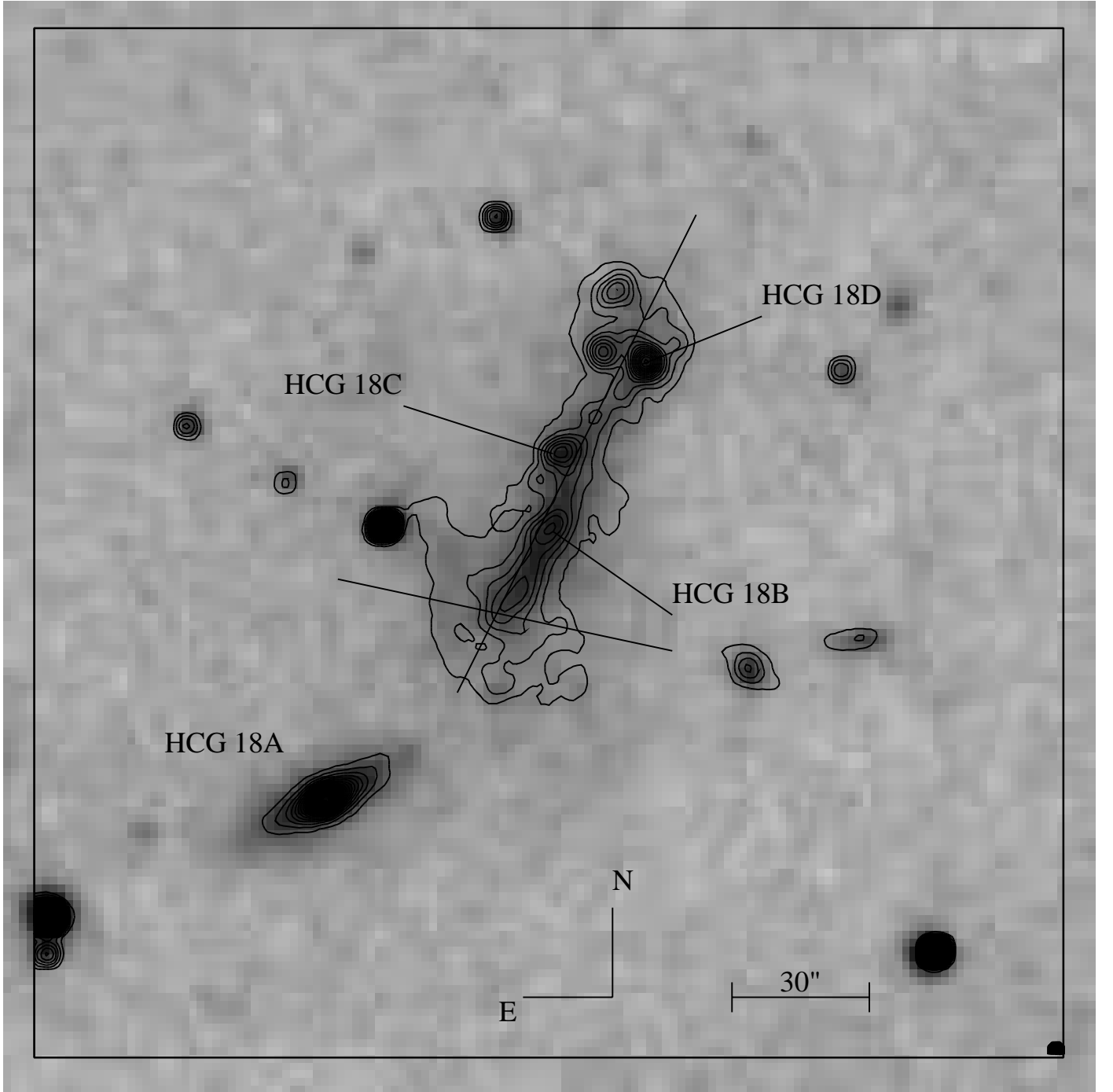


FIG. 1.— Continuum image of H18a, b, c and d. The contours (in arbitrary units) were plotted after a rectangular smoothing with a box of 5×5 pixels. The continuum map has been superimposed to a DSS image. We also show the three directions, one east - west (on the southern region), one north - south along the group major axis and one coinciding with the HI major axis ($PA=20^\circ$). These axis were used for deriving the LOS velocity curves shown in Fig.4.

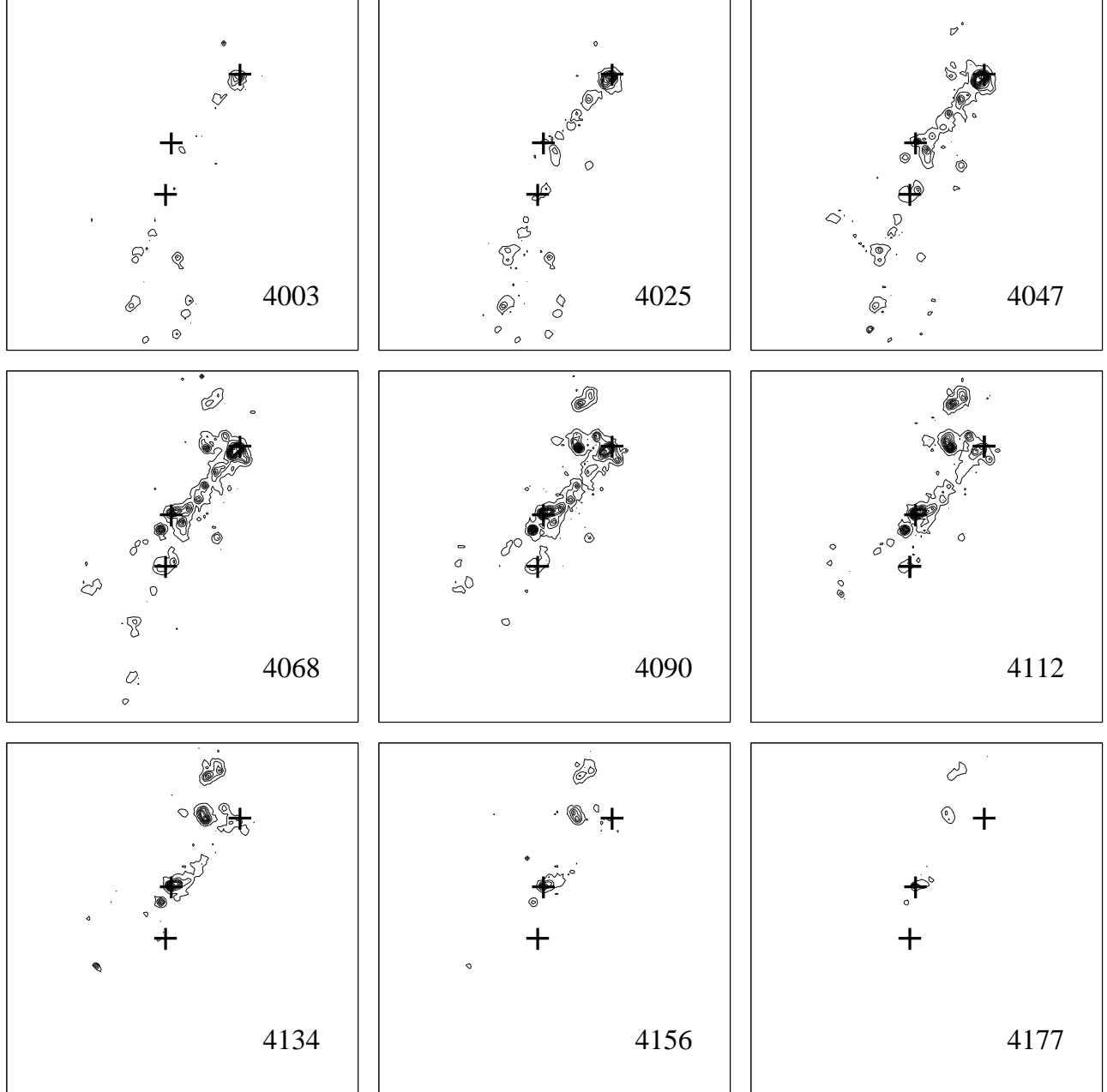


FIG. 2.— Channel maps of H18. We present 9 of the 24 channels we have scanned. The field of view is $1.8' \times 1.8'$, North is up and East is to the left. Crosses represent the positions of H18b, c and d. In each panel we mark the velocity of the channel. The lowest isointensity represents a flux density of $4.4 \times 10^{-16} \text{ erg s}^{-1} \text{ cm}^{-2} \text{ arcsec}^{-2}$.

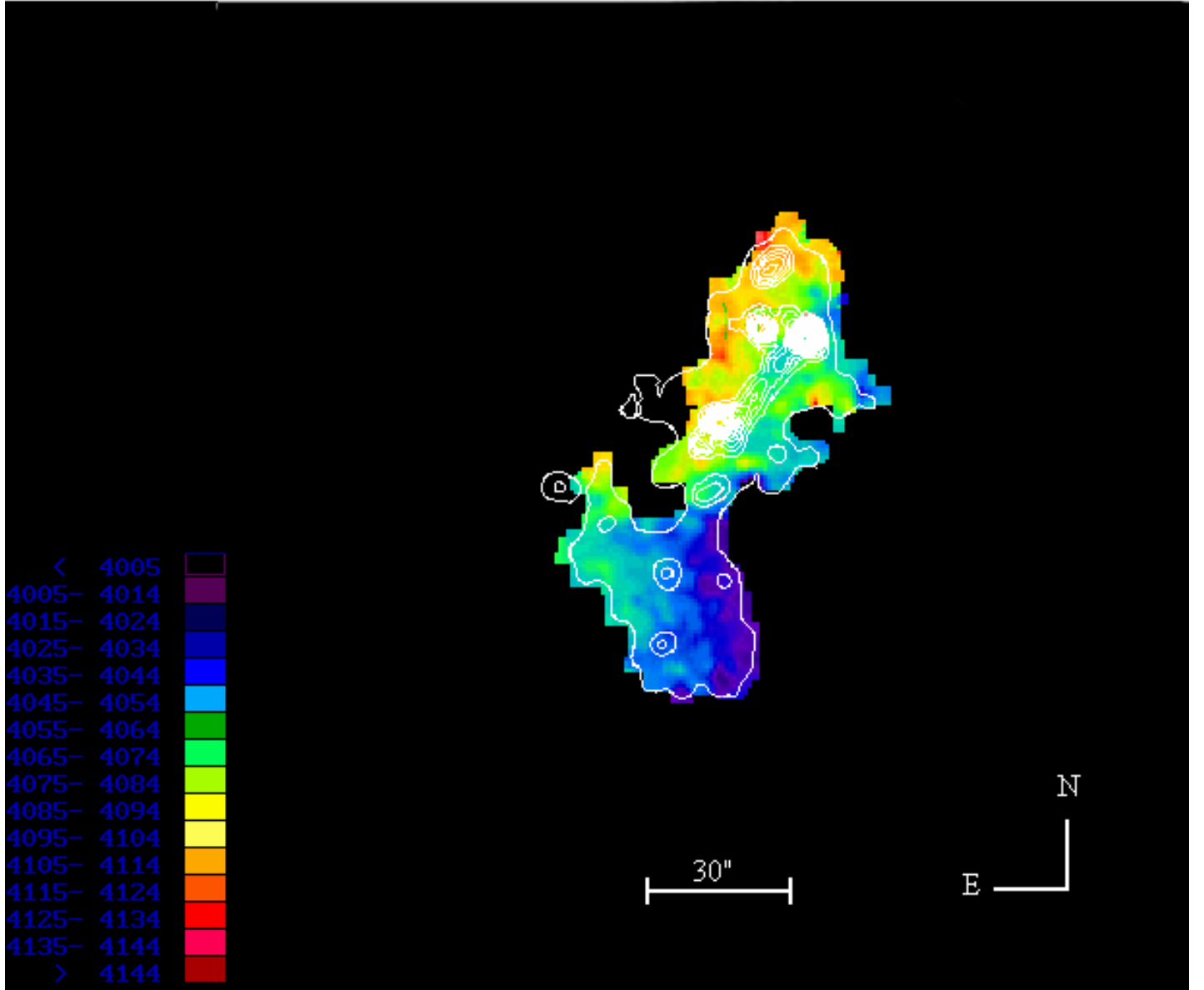


FIG. 3.— Velocity field of H18. We present the velocity map of the group and, superimposed with white isophote, the H α integrated flux map (See Fig. 5). Velocity map has been spacialy smoothed with a box of 3×3 pixels.

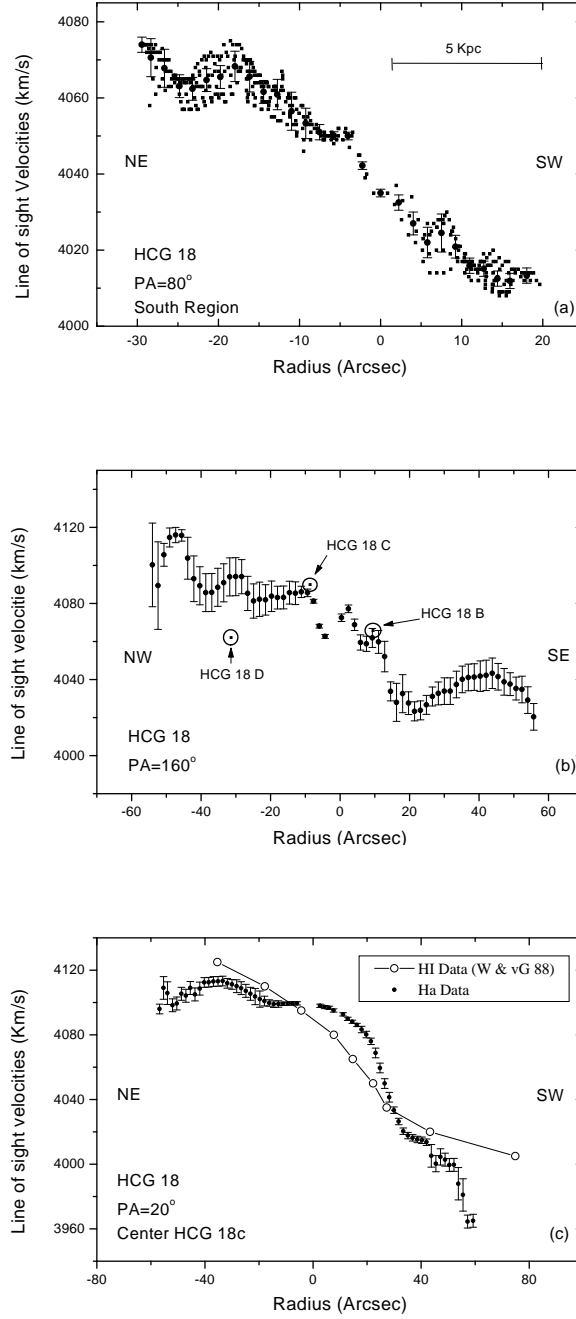


FIG. 4.— Line of sight velocity curves of HCG 18. In all plots, filled circles represent the average values of velocities in a 2×2 pixels crown with the dispersion error bars indicated. (a) Velocity curve of the southern region of the group, along an axis with a PA= 80° (see fig. 1 for the exact location of the axis). The plot shows all the points inside a cone with an half angle at the summit of 20° . (b) Line of sight velocities along the major axis of HCG 18 (PA= 160°). The positions of the three group members, HCG 18b, c and d are marked. (c) This plot shows the velocity curve across an axis with a PA= 20° using the velocity field presented on fig. 6 (at the resolution of HI data). Overplotted are the data points taken from the VF of Williams & van Gorkom (1988) along the same PA of 20° .

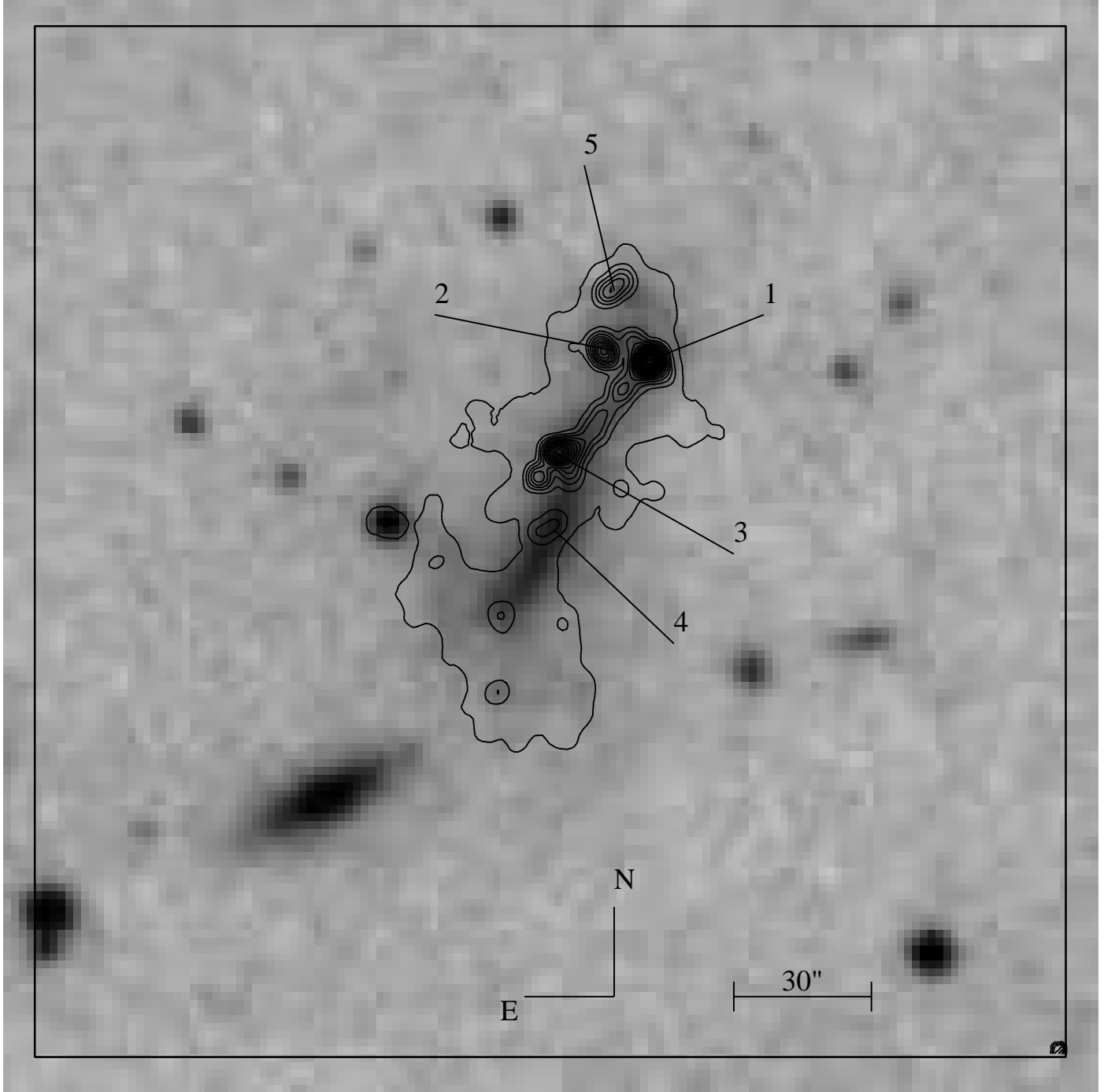


FIG. 5.— the $H\alpha$ integrated flux map of HCG 18. The map has been spatially smoother with a rectangular box of 5×5 pixels. Isointensities are in unit of $10^{-16} \text{ erg s}^{-1} \text{ cm}^{-2} \text{ arcsec}^{-2}$. The lowest level is 1.1 and step the is 5. The monochromatic image has been superimposed to a DSS image.

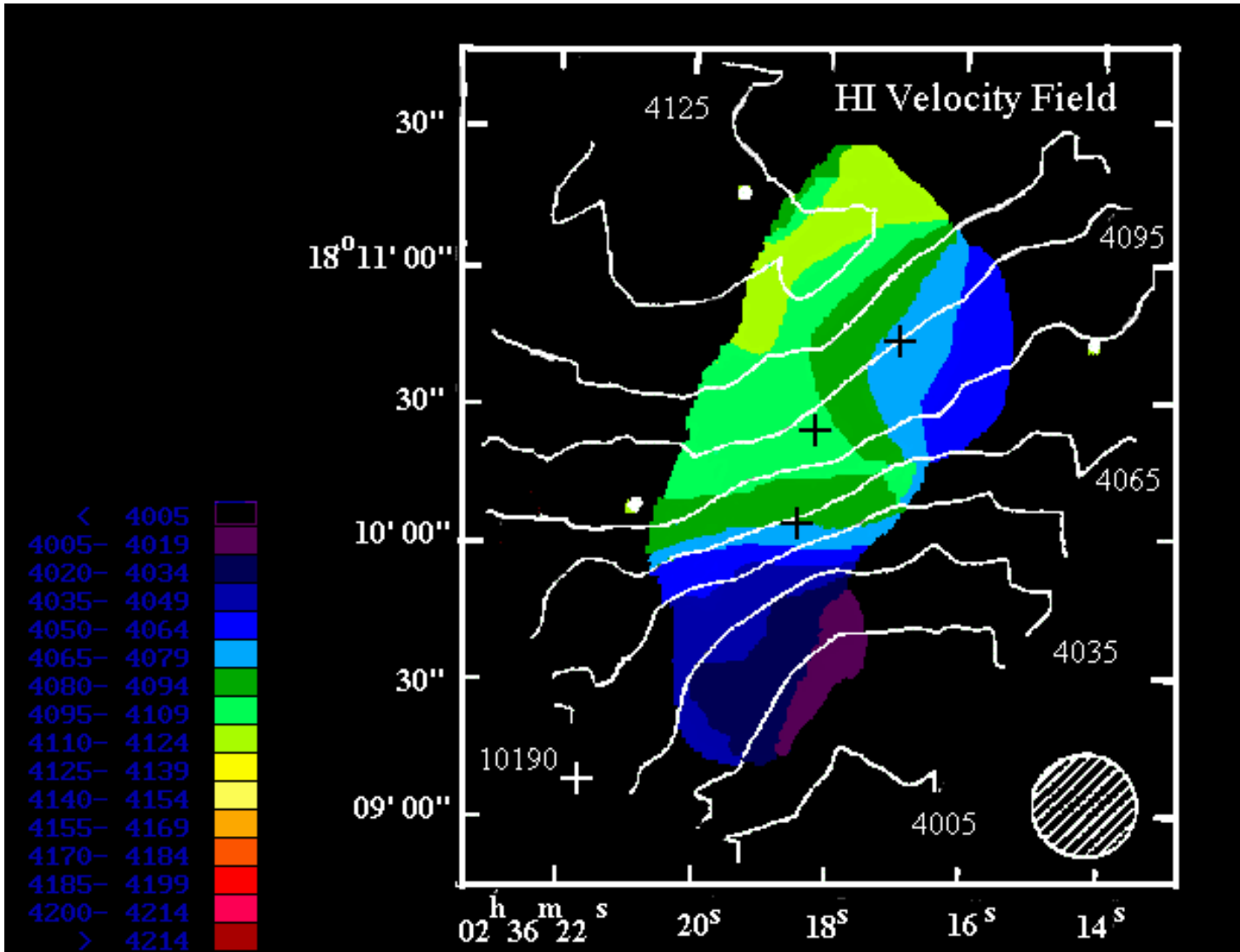


FIG. 6.— Superposition of the HI velocity map from Williams & van Gorkom 1988 on our H α VF. In order to match the resolution of the two maps, we performed a gaussian smoothing of 22'' (see text). The crosses represent positions of group members b, c and d.